PERGAMON

International Journal of Heat and Mass Transfer 42 (1999) 555–564

International Journal of HEAT and MASS TRANSFER

Oscillatory thermocapillary flows in open cylindrical containers induced by CO_2 laser heating

Y. Kamotani*, S. Ostrach, J. Masud

Department of Mechanical and Aerospace Engineering, Case Western Reserve University, Cleveland, OH 44106, U.S.A.

Received 30 December 1997; in final form 14 April 1998

Abstract

Oscillatory thermocapillary flow experiments were conducted in microgravity. Silicone oil was placed in cylindrical containers and heated at the center by a CO_2 laser beam. The main objectives were to determine the onset of oscillatory thermocapillary flow and to study the important features of the oscillatory flow. Numerical and scaling analyses were also performed to understand the basic steady flows. The onset conditions show that the oscillation phenomenon cannot be explained if the fluid-free surface is assumed to be undeformable. Therefore, a parameter representing free surface deformation is derived. The oscillation patterns and frequencies are also presented.

Nomenclature

Ar container aspect ratio, H/R
a absorption length of CO_2 laser by test fluid
C_p specific heat at constant pressure
D container diameter
f oscillation frequency
f^* dimensionless oscillation frequency defined by equation (12)
H container depth
Hr relative heating zone size, R_h/R
k thermal conductivity
Ma Maragoni number based on ΔT, $\sigma_T \Delta T R/\mu_c \alpha$
Ma_Q Marangoni number based on Q, $(\sigma_T Q/k\mu_c\alpha)^{2/3}$
$(Ma_Q)_{cr}$ critical Ma_Q for onset of oscillations
Pr_m Prandtl number evaluated at temperature $(T_H+T_C)/2$, $\mu_m C_p/k$
Pr_C Prandtl number evaluated at temperature T_C, μ_c C_p/k
Q total heat input
Q_{cr} critical heat flux for onset of oscillations
(r,z) cylindrical coordinate system defined in Fig. 1
R container radius
R_h heating zone radius
R_σ^* surface-tension Reynolds number based on $R_h, \rho\sigma_T\Delta T R_h/\mu_m{}^2$
S S-parameter defined in equation (11)
T temperature
T_C side (cold) wall temperature
T_H free surface temperature at center
U_b velocity of bulk flow
U_0 maximum velocity in heated region.

Greek symbols

α thermal diffusivity
ΔT overall temperature difference, $T_H - T_C$
ΔT_b temperature difference for bulk flow
δ_s free surface deformation in heated region at onset of oscillations
δ_{TH} thermal boundary layer thickness in heated region
δ_{TS} thermal boundary layer thickness along free surface
μ_c fluid viscosity evaluated at temperature T_C
μ_m fluid viscosity evaluated at temperature $(T_H+T_C)/2$
ρ fluid density
σ surface tension
σ_T temperature coefficient of surface tension
Ψ_{max} maximum stream function.

1. Introduction

Thermocapillary flows are known to become oscillatory (time-periodic), but how and when they become

* Corresponding author. Tel.: 001 216 368 6455; Fax: 001 216 368 6445; E-mail: yxk@po.cwru.edu

0017–9310/98 $19.00
PII: S0017–9310(98)00163–X

oscillatory in containers of unit-order aspect ratio is not yet fully understood. The present work is a part of our continuous effort to obtain a better understanding of the phenomenon. Our past work on the subject as well as related studies by other investigators have been reviewed [1–3].

Thermocapillary flow experiments in normal gravity are limited to a narrow parametric range so as to minimize gravity and buoyancy effects, which is an important reason for our lack of understanding of the oscillation phenomenon. One important unanswered question is what role, if any, free surface deformation plays in the oscillation mechanism. For that reason we performed thermocapillary flow experiments, called the Surface Tension Driven Convection Experiment-2 (STDCE-2), aboard the USML-2 Spacelab in 1995. The main objectives of the experiments were to investigate oscillatory thermocapillary flows in microgravity and to clarify the importance of free surface deformation in such flows. The experiments were conducted over a wide range of conditions. Some important data are presented, analyzed and discussed herein.

2. Description of experiments

The experimental arrangement for STDCE-2 is sketched in Fig. 1. The hardware and its performance during flight are described in detail by Pline et al. [4]. Open circular containers of inner diameters 1.2, 2.0 and 3.0 cm were used. The container side wall was made of copper and was maintained at a uniform temperature by coiling a cooling water loop around it. The cooling water interfaced with the Spacelab water through a heat exchanger, which kept the side wall temperature at around 14°C during the tests. The bottom wall was made of Teflon. The test fluid was 2 centistokes silicone oil. Its pertinent properties can be found in the report by Lee et al. [5]. A small amount of Pliolite particles (~ 70 μm size) were mixed in the test fluid for flow visualization purposes. A laser diode light source illuminated the whole flow field. A CCD camera recorded the particle motions. The test fluid was heated at the center by a carbon dioxide laser beam. Its diameter was varied by a lens system (Fig. 1). The beam had an axisymmetric Gaussian profile. The absorptivity of the laser beam by the test fluid was determined to be 0.9 [6].

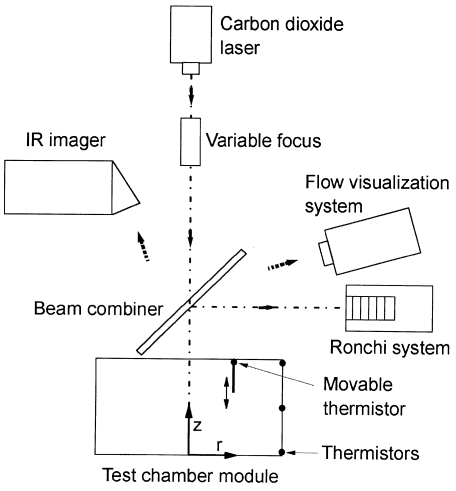

Fig. 1. Experimental arrangement of STDCE-2.

Three thermistors were imbedded along the side wall to monitor its temperature. In addition, one thermistor each monitored the bottom wall temperature and the air temperature above the test fluid. One thermistor probe was placed in the fluid. The probe was located at the half-radius point of the container and movable in the axial direction (Fig. 1). The probe was lowered to the bottom plate when the onset of oscillations was determined so as to avoid its interference with the onset.

An infrared imager (IR imager) operating in the 8–14 μm wavelength range was used to construct the thermograms of the free surface. The same system was used in our earlier space experiments [1–3] except for a zoom telescope used in the present experiments to view smaller containers. Radiation absorption length of the test fluid in the above wavelength range has been measured to be 0.02 mm [6]; so the imager detects radiation from the liquid layer of about that thickness below the free surface.

Free surface shape and motion were measured optically by a Ronchi system. The system used in STDCE-2 is described in detail by Stahl and Stultz [7]. The Ronchi data are still being analyzed so that results are not presented herein. Important to the present work is that the system was used to determine flatness of free surface within 0.1 mm before each experiment.

The resolution of the laser power was 0.01 W, and the power output fluctuation was less than 1% of the set point (usually less than the resolution). The critical heat flux for onset of oscillations was determined within 0.02 W. The accuracy of the thermistor readings was 0.1°C, which was also the resolution of thermistor data digitization. The side wall temperature nonuniformity was within the thermistor resolution. Error in oscillation frequency measurement was $\pm 10\%$.

A typical experimental procedure was carried out in the following manner. Before each test, the test fluid, kept in a reservoir, was pumped slowly into the test chamber through a filling hole at the bottom. The chamber was filled until the free surface became flat, as determined by the Ronchi system. Then, the CO_2 laser was turned on. In almost all tests the laser power was increased stepwise by manual operation. At each power setting, flow and thermal fields were checked carefully for the onset of oscillations. Power was increased after the flow field was

judged to be steady. Typically power was changed after 2–3 min. Video information from the three diagnostic techniques (flow visualization, infrared imager and Ronchi system) was downlinked in real time to the ground station where several scientists monitored the experiment, so that we were all involved in determining the onset of oscillations by detecting small but systematic changes in those images. After finding the onset point of oscillations, the laser power was increased until oscillations were very pronounced, and flow and temperature fields of the oscillatory flow were then investigated. After each test the fluid was withdrawn to the reservoir. The whole process took about 2 h.

3. Ranges of parameters

As discussed in our earlier work [1, 2], the important dimensionless parameters for steady thermocapillary flows in the present experimental configuration with a flat free surface are: Marangoni number (Ma), Prandtl number (Pr), container aspect ratio (Ar), and relative heating zone size or heater ratio (Hr). Heat loss from the free surface is due to radiation and the forced convection within the surrounding air induced by the free surface motion. Based on the numerical analysis to be discussed later, heat loss from the free surface relative to the total heat transfer rate is estimated to be about 3% so that it is not a major factor in the present experiments. The mean absorption length of CO_2 laser by the test fluid has been determined to be $a = 0.06$ mm. The ratio a/R_h ranges from 0.02 to 0.2 in the present experiment. The effect of this parameter will be discussed later.

For a given configuration and fluid, thermocapillary flow is known to become oscillatory beyond a certain ΔT. If the above list of parameters is sufficient to describe the onset of oscillations, Ma should specify the onset, since Ma is the only major parameter containing ΔT. However, we have shown in various configurations that Ma alone cannot specify the onset condition. Although we have conducted ground-based experiments in the present laser heating configuration, the data were taken in a limited range of Ma in order to minimize buoyancy effects. Therefore, the present work is designed to check the validity of that statement over a wider range in microgravity and then, to find an additional parameter to describe the onset.

Fourteen flat surface tests were performed in the laser heating mode. Parametric ranges of those tests near and above the onset of oscillations were: $Ma > 4 \times 10^4$, $Pr_m = 22$–32, $Pr_C = 33$, and $Hr = 0.05$, 0.1 and 0.2. Eleven tests were conducted with $Ar = 1$. In the other three tests a cylindrical plastic disc was inserted at the bottom of each test chamber to reduce its aspect ratio to 0.5. The above Ma is based on ΔT, which is convenient because Ma is defined similarly in other configurations. Later, Ma based on Q will also be introduced.

4. Numerical analysis

To supplement the experimental work the basic steady flow fields were analyzed numerically. The numerical scheme has been described in our earlier work [1, 2], so it is described only briefly. The coordinate system is defined in Fig. 1. The velocity and stream function are non-dimensionalized by $\sigma_T \Delta T/\mu_c$ and $\sigma_T \Delta T R H/\mu_c$, respectively. The temperature is made dimensionless as $(T - T_C)/\Delta T$. Fluid properties are taken to be constant except for viscosity and surface tension which vary with temperature. The free surface is assumed to be non-deformable in this steady flow analysis.

The present scheme is based on the SIMPLER algorithm. A non-uniform grid system is employed with the smallest meshes next to the free surface and also next to the cold wall. For conditions of $Ma = 4.3 \times 10^4$ (close to the largest value for the steady flow in the experiments), $Hr = 0.2$, and $Ar = 1$, the values of $k\Delta T R_h/Q$ (dimensionless ΔT) computed with three different grids, 37×31 ($r \times z$), 46×40 and 67×60 with the smallest axial mesh sizes next to the free surface of 0.003, 0.001 and 0.0005, respectively, are 0.0114, 0.0110 and 0.0110. The computed maximum stream functions are 0.00221, 0.00218 and 0.00217, respectively. Therefore, the 46×40 grid is used in the present analysis.

5. Basic flow fields

The basic steady flow fields are discussed first based on numerical and scaling analysis. Typical streamlines and isotherms are shown in Fig. 2 for two values of Ma (the larger Ma is near the onset of oscillations in the STDCE-2 experiment and the smaller one is for a viscous-dominated flow). The main flow structure in unicellular, which agrees with our experimental observations. With increasing Ma, the center of cellular motion shifts slightly toward the cold wall. The shift is due to weak inertia forces. Inertia forces are mainly important in the relatively small heated region. In the bulk flow the inertia effect is less important so that a velocity boundary layer does not appear along the free surface (the cell center simply shifts in the r-direction while keeping its z-location nearly fixed at about $z/H = 0.8$). One important feature of the thermal field is that there exists a very thin thermal boundary layer along the free surface, especially in the heated region, because Ma is large. Consequently, a large temperature drop occurs in the heated region and the bulk fluid outside the boundary layer remains relatively cool.

Because of the large thermocapillary driving force in

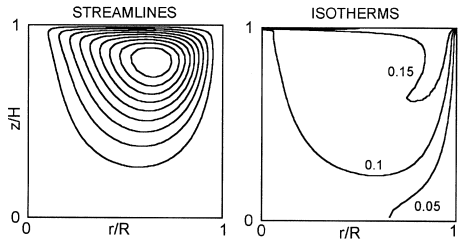

(a) Streamlines and isotherms for Ma = 9.2 x 10^4 (Ma_Q = 1.0 x 10^4)

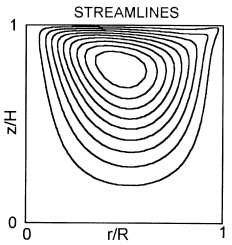

(b) Streamlines for Ma = 8.1 x 10^3 (Ma_Q = 1.3 x 10^3)

Fig. 2. Basic flow and temperature fields ($Ar = 1$, $Hr = 0.1$ and $Pr_C = 33$).

the heated region the fluid velocity along the free surface increases sharply in the radial direction and attains the maximum value at the edge of the heated region [8]. According to Kamotani et al. [8], if R_σ^*, the surface tension Reynolds number based on R_h and ΔT, is larger than about 150, both velocity and temperature boundary layers exist in the heated region and the dimensionless maximum velocity in the region (U_0) scales as

$$\frac{\mu_m U_0}{\sigma_T \Delta T} \sim \left(R_\sigma^*\right)^{(-1/3)} \tag{1}$$

The range of R_σ^* was $R_\sigma^* > 280$ in the STDCE-2 tests, and R_σ^* was larger than 160 in our earlier ground-based experiments with 2 centistokes silicone oil, so we were near the beginning of the boundary-layer regime in those tests. The temperature field in the heated region is influenced by the CO_2 laser absorption length (a). For a given Q, the maximum surface temperature (or ΔT) decreases with increasing a/R_h, as more fluid volume is heated by the laser. For example, for the conditions of $D = 2.0$ cm, $R_h = 0.1$ cm ($Hr = 0.1$) and $Q = 0.15$ W, the values of ΔT will change from 14.7 to 9.6°C when a/R_h is varied from 0.02 to 0.2 (the range of a/R_h in the STDCE-2 tests).

The free surface temperature was measured by the IR imager in STDCE-2. Computed surface temperature distributions and the imager data agreed generally well except in the heated region where the imager data are slightly lower than the computed value because of the thin thermal boundary layer [9].

Since the mass flux out of the heated region is confined to the thin boundary layer, its total mass flux is relatively small compared to that of the bulk flow. The bulk flow is driven mainly by the surface temperature gradient outside the heated region. The characteristic temperature drop in the bulk flow (ΔT_b) can be estimated as follows. The laser heat absorbed in the heated region is convected from that region to the cold wall through a thermal boundary layer along the free surface, which gives the following relation,

$$Q \sim \rho C_p U_b \Delta T_b \delta_{TS} R \tag{2}$$

where δ_{TS} is the thermal boundary layer thickness along the free surface and is estimated as

$$\delta_{RS} \sim \left(\frac{\alpha R}{U_b}\right)^{1/2} \tag{3}$$

Equation (2) is independent of the heating zone diameter (and the laser absorption length), because all the heat from the laser goes into δ_{TS} regardless of diameter. As mentioned above, the axial position for the center of unicellular motion is nearly fixed (at about $z/H = 0.8$) in the parametric range of the present study. Therefore, assuming that the overall axial extent of the bulk flow scales with the container dimension (or the bulk flow is viscous-dominated), the shear stress balance at the free surface gives for $Ar = 1$

$$U_b \sim \frac{\sigma_T \Delta T_b}{\mu_c} \tag{4}$$

As the isotherms of Fig. 2 show, the bulk flow temperature is close to the cold wall temperature, so the viscosity associated with the bulk flow is evaluated at T_C. Since the bulk flow region occupies a much larger area than the heated region, the maximum stream function is determined by the bulk flow so that $\Psi_{MAX} U_b R^2$ for $Ar = 1$. Then, from equations (2)–(4) one obtains

$$\frac{\Psi_{max}}{\alpha R} \sim \left(\frac{\sigma_T Q}{k \mu_c \alpha}\right)^{2/3} \tag{5}$$

The right side of equation (5) is the Marangoni number based on ΔT_b and R, called Ma_Q herein

$$Ma_Q = \frac{\sigma_T \Delta T_b R}{\mu_c \alpha} = \left(\frac{\sigma_T Q}{K \mu_c \alpha}\right)^{2/3} \tag{6}$$

The scaling law, equation (5), is compared with the numerical results in Fig. 3. The numerical results are obtained for a range of Ma_Q up to near the onset of oscillations found experimentally. The scaling law agrees very well with the computed results. It is important to note for a later discussion that the proportionality constant for equation (5) is rather small, about 0.01 according to Fig. 3, which reflects mainly the fact that the thermocapillary force does not act uniformly over the free surface. Since $\Psi_{max} \sim U_b R^2$, U_b and Ψ_{max} are proportional so that the proportionality constant for U_b in equation (4) is also about 0.01.

The Reynolds number of the bulk flow can be estimated as $\rho U_b R/\mu_c \sim \rho \Psi_{max}/\mu_c R$, which is less than about

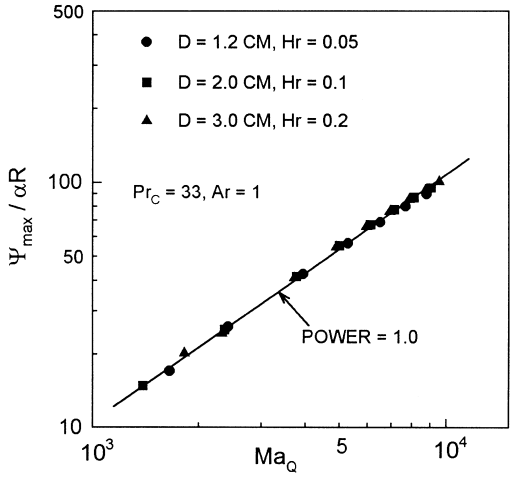

Fig. 3. Scaling law for maximum stream function.

3 near the onset of oscillations. Therefore the bulk flow Reynolds number is not large enough to have a boundary-layer type flow. It can be shown that the ratio of the volume flux out of the heated region ($U_0\delta_v R_h$ where δ_v is the velocity boundary layer thickness in the heated region) to the bulk flow volume flux ($U_b R^2$) is expressed as $(R_\sigma^*)^{1/3} Pr_m Hr/Ma_Q$. The ratio is less than 1% near the onset of oscillations. Therefore, all the assumptions made in the above analysis are consistent with the results. In summary, the bulk flow driven by ΔT_b dominates the overall flow and is viscous-dominated in the parametric ranges of the present experiments. For that reason, we use Ma_Q to characterize the bulk flow in the following discussion.

6. Oscillatory flows

When the flow was steady, the tracer articles were observed to recirculate in fixed radial planes (*rz*-planes in Fig. 1) but beyond a certain Q the particles started to move back and forth in the azimuthal direction in a toroidal spiral, which was the onset of oscillations. The oscillatory flow structure is similar to the one observed in normal gravity, which was discussed by Lee et al. [5]. The isotherms obtained from the IR images during one cycle of oscillations are given in Fig. 4. Since the IR imager cannot accurately resolve the surface temperature near the heated region, as discussed above, Fig. 4 is meant to show only qualitative pattern changes during oscillations. When the flow was steady, the isotherm pattern was nearly axisymmetric. When the flow became oscillatory, the pattern became elongated, the elongation direction changing alternately between two nearly perpendicular directions (Fig. 4). Increasing Q beyond the critical value did not alter this pulsating pattern. With those pattern changes in one cycle of oscillations, the free surface temperature along a given radial direction becomes alternately high and low, which is important for the oscillation mechanism to be discussed later. The period in which the surface flow is relatively warm is called the active period and the period of relatively cold surface flow is called the slow period herein.

The heat input at the onset of oscillations is called critical heat flux (Q_{cr}). The critical heat fluxes measured in the tests with $Ar = 1$ are presented in Fig. 5, together with data taken in our ground-based tests with smaller containers filled with the same fluid [5]. The flow was found to be already oscillating at the minimum power of the CO_2 laser for the 1.2 cm container, so that the critical heat flux could not be determined for that container. As seen in Fig. 5, the trend of the space data is consistent with that of the ground data: Q_{cr} increases with increasing D. Although not shown here, data taken in tests with submerged heaters show that the critical temperature difference for the 1.2 cm container measured in STDCE-2 was close to that measured in 1 g with the same container, which means that buoyancy has negligible effect on the onset condition in our ground tests with small containers ($D \leqslant 1.2$ cm). According to Fig. 5, Q_{cr} seems to depend slightly on Hr but the effect of Hr is within the experimental error.

Based on the critical heat flux for onset of oscillations, we compute $(Ma_Q)_{cr}$ according to equation (6). The result is given in Fig. 6. As in our past work, we plot $(Ma_Q)_{cr}$ against D, since D is the only main quantity varied in those tests. If $(Ma_Q)_{cr}$ is the only parameter to specify onset of oscillations, it should not vary with D. Figure 6 shows that, as we have found also in various other experiments under different conditions, the critical Marangoni number varies with container size. Clearly, Ma along cannot specify the onset. A new aspect and parameter must be introduced.

Based on our extensive experimental and theoretical work on the oscillation phenomenon, we believe that this additional aspect is free surface deformation. Our physical model of oscillations is given below. In the following discussion, flow along the free surface is called the surface flow and that toward the heated region in the interior is called the return flow. Although the heated region is a relatively small region, it is an important region because that is where hot fluid originates. Therefore what happens there could influence the entire temperature field. The heated region is sketched in Fig. 7a. The important features of the present configuration are that the heated region is relatively small ($Hr < 1$) and that the fluid velocity there is large. Consequently, the convection time scale in this region is small relative to the overall convection time. The small convection time means that the temperature field, and thus the thermocapillary driving force, could change very quickly.

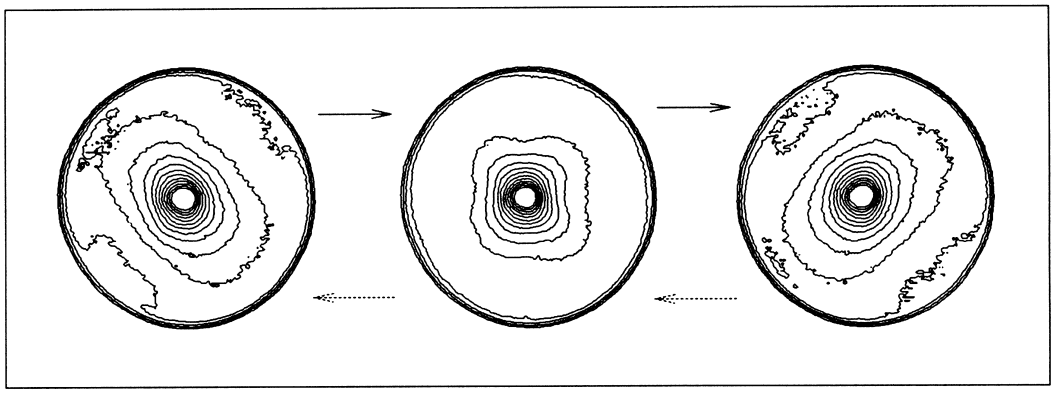

Fig. 4. Isotherms obtained from thermograms taken during oscillations ($Ma_Q = 2.4 \times 10^4$, $Ar = 1$ and $Hr = 0.1$).

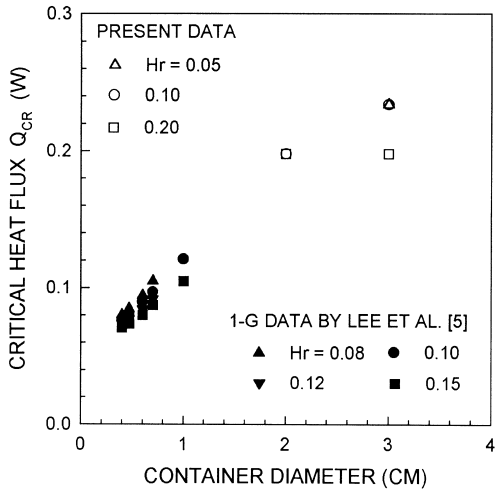

Fig. 5. Critical heat fluxes measured in 1 g and in microgravity for $Ar = 1$.

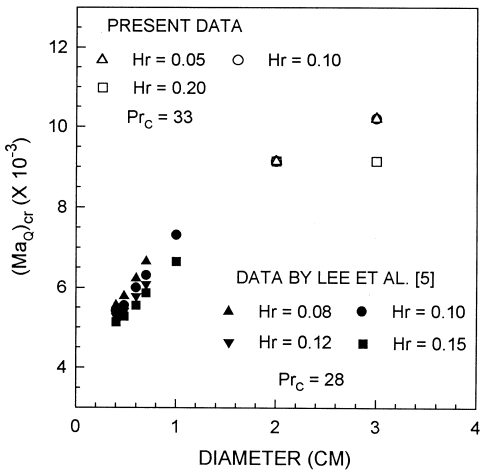

Fig. 6. Critical Marangoni numbers for onset of oscillations for $Ar = 1$.

Therefore, when the surface flow in the heated region is changed quickly, the return flow would not respond immediately, because the free surface must deform first to generate sufficient pressure gradient for the response, in other words there exists a time lag. This time lag is the primary factor in the oscillation mechanism.

Suppose that the surface flow in the heated region is increased by a small amount. The return flow in that region does not respond immediately because the free surface must deform first (the surface must depress). Because of the deformation a small amount of the fluid is removed from the surface region, which decreases the thermal boundary layer thickness in the heated region, as illustrated in Fig. 7a. Then the radial temperature gradient in the boundary layer increases as a result of increased cooling of the layer by axial conduction (See Fig. 7b). The increased radial temperature gradient, in turn, further increases the surface flow. The trend continues until the return flow catches up with the surface flow. This marks the beginning of an active period. Around this time, the flow becomes non-axisymmetric: the active period occurs only in diametrically opposed regions at a given time, as the IR images in Fig. 4 show. This non-axisymmetry is caused by the fact that the surface temperature reduction in the heated region (Fig. 7b) induces azimuthal temperature gradients in this region. Consequently, more heat is convected to the active region from other directions by the thermocapillary flow caused by the azimuthal temperature gradients.

As more heat is transported out of the heated region, the surface temperature just outside the region increases (Fig. 7b). Subsequently the hot region propagates toward

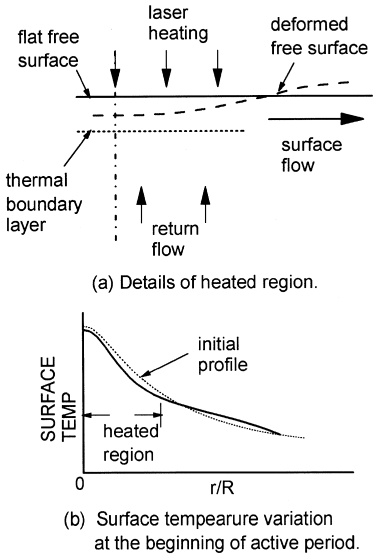

Fig. 7. Sketch of heated region and variations of free surface and surface temperature at the beginning of active period.

the cold wall, driven by the radial temperature gradient near its front. This convection of hot fluid toward the cold wall is clearly seen in the IR images. After the hot fluid reaches the cold wall, it then comes back to the heated region as the return flow. Therefore, after some time, which is proportional to the bulk flow convection time, the return flow begins to warm the heated region. As a result, the surface temperature there begins to rise, which reduces the aforementioned azimuthal thermocapillarity toward the active region. Consequently, the heat flux in the active region is reduced and the surface temperature outside the heated region decreases. This is the slow period in that region. In the mean time, the heat flux in the originally slow region begins to increase and by the same mechanism described above, that region now becomes active and goes through the same cycle.

The above discussion suggests that the flow becomes oscillatory when the free surface deformation in the heated region becomes large compared to the thermal boundary layer thickness in this region so that the thermocapillary driving force there is substantially altered. Therefore, a parameter, which characterizes that ratio, is derived.

The free surface deformation of interest, δ_s, can be estimated as follows. Since the surface flow is limited to a thin boundary layer in the heated region, the pressure change and the associated free surface deformation in the region are caused by the bulk flow with velocity scale U_b. With deformation δ_s in the heated region, the pressure of order $\sigma\delta_s/R_h^2$ is created in the heated region, which produces the pressure gradient of order $(\sigma\delta_s/R_h^2)/R$ in the bulk flow toward the heated region. Suppose that the increased surface velocity causes the free surface to recede with a velocity of order U_b in the heated region. Then the deformation causes a time lag of order δ_s/U_b because it takes that long to deform the surface. After the time lag the bulk flow responds to the above pressure gradient and stops the receding surface, which can be written mathematically as

$$\rho\frac{U_b}{\delta_s/U_b}\sim\sigma\frac{\delta_s}{R_h^2}\frac{1}{R} \tag{7}$$

Equation (7) is a balance of the unsteady term and the pressure gradient in the momentum equation. Justification for using the unsteady term will be given later. The thermal boundary layer thickness in the heated region can be estimated as

$$\delta_{TH}\sim\left(\frac{\alpha R_h}{U_0}\right)^{1/2} \tag{8}$$

Based on our concept of oscillations the ratio of δ_s to δ_{TS} must be on the same order for the oscillations to start. From equations (1)–(8) one obtains

$$\frac{\delta_s}{\delta_{TH}}\sim\left(\frac{\rho\alpha^2}{\sigma R}\right)^{1/2}Ma_Q(R\sigma^*)^{1/3}Pr_m^{1/2} \tag{9}$$

The above ratio is called a surface deformation parameter or S-parameter. Oscillations should appear beyond a certain value of S.

Based on the above results, the deformation time δ_s/U_b relative to the diffusion time scale R^2/υ can be expressed as $(\rho\alpha^2/\sigma R)^{1/2}PrHr$. The ratio is much less than unity in all of our experiments, both in microgravity and on the ground. This is the reason why the unsteady term is used in equation (7).

In order to evaluate R_σ^* and Pr_m in equation (9) one needs to know ΔT. As explained earlier, it is very difficult to measure the free surface temperature at the center (T_H) accurately because of the very thin thermal boundary layer in the heated region. Although T_H can be determined approximately from the IR imager data in the STDCE-2 tests, we could not do so in our ground-based tests with smaller containers (R less than 5 mm) because the boundary layer was too thin. Therefore, we relate ΔT to Q so that the S-parameter can be evaluated in terms of imposed quantities in the following

Neglecting the effect of absorption length we can relate Q and ΔT from a balance between heat input and conduction heat transfer in the heated region [8].

$$\frac{Q}{k\Delta TR_h}\sim\frac{R_h}{\delta_{TH}} \tag{10}$$

The error due to neglecting the absorption length will be discussed later. Then from equations (1), (8) and (10) one can relate Q and ΔT. The S-parameter can then be expressed as

$$S = \left(\frac{\rho\alpha^2}{\sigma R}\right)^{1/2} Ma_Q^{11/8} Pr_c^{1/8} \left(\frac{\mu_c}{\mu_m}\right)^{1/8} \tag{11}$$

The viscosity ratio factor in equation (11) can be set to one generally. Then we can compute S without measuring ΔT. The absorption length affects the relationship between Q and ΔT, but since ΔT appears mainly as $(R\sigma^*)^{1/3}$ in equation (10), its effect on S is relatively small. Based on the numerical analysis for the conditions of the STDCE-2 and our ground-based tests, it is estimated that the error of neglecting the absorption length and using equation (10) in the computation of S is $\pm 11\%$.

The data in Fig. 5 are replotted in Fig. 8 were S is computed according to equation (11). As seen in the figure, all the data are correlated very well with the S-parameter: all the data lie within $S = 69 \pm 14\%$. The data scatter is largely due to the effect of absorption length. Therefore, one can say that the flow becomes oscillatory when S is larger than about 70. It is clear that Ma_Q is an important parameter, because the oscillation are a convection phenomenon, but in the parametric ranges of STDCE-2 and our ground tests the S-parameter is the limiting parameter. The reason why the magnitude of S is much larger than unity is that S is proportional to $U_b^{11/8}$, equation (11), and, as mentioned earlier, we need to multiply U_b by a factor of approximately 0.01 to estimate its magnitude properly. If we include the multiplication factor, the magnitude of S will be of order unity. It can be shown that computing S according to equation (9) with the measured or computed ΔT can reduce the scatter in Fig. 8. However, a large amount of data available for the onset of oscillations in the so-called half zone configuration show that the data tend to scatter considerably for various reasons [10]. Therefore, it is not attempted here to include the effect of absorption length in S.

The oscillation frequencies are shown in Fig. 9. Only a few data are available from our ground-based tests. The frequencies were determined from the videotapes of IR images and flow visualization. Except for the data for $D = 1.2$ cm, the oscillations frequencies were obtained near the onset of oscillations. The frequency decreases with increasing D. The frequency is not a strong function of Hr. According to the aforementioned model for oscillations, the oscillation period is associated with the overall time of convection, R/U_b. Therefore, the oscillation frequency is non-dimensionalized herein as

$$f^* = \frac{f}{U_b/R} = \left(\frac{fR^2}{\alpha}\right) \Big/ Ma_Q \tag{12}$$

Since the scaling law of U_b used in equation (12) is obtained for the basic steady flow, the above expression is valid only near the onset of oscillations. The dimensionless frequencies are presented in Fig. 9. The figure shows that f^* is nearly constant (about 0.018) in agreement with equation (12). The values for $D = 1.2$ cm are generally smaller than those for other containers, which is due to the fact that the oscillatory flow was not close to the onset.

The critical heat fluxes for the onset of oscillations for the shallow containers ($Ar = 0.5$) are given in Fig. 10. Only three data points were obtained in STDCE-2 and no 1 g data are available for $Ar = 0.5$. Compared to the critical values for $Ar = 1$ (Fig. 5), the values for $Ar = 0.5$ are about twice as large for a given container diameter.

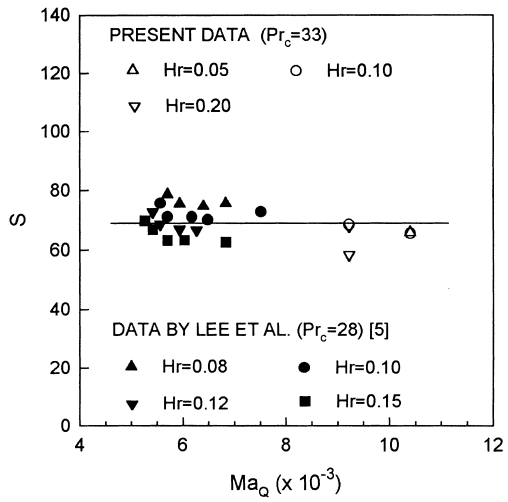

Fig. 8. S-parameter for onset of oscillations for $Ar = 1$.

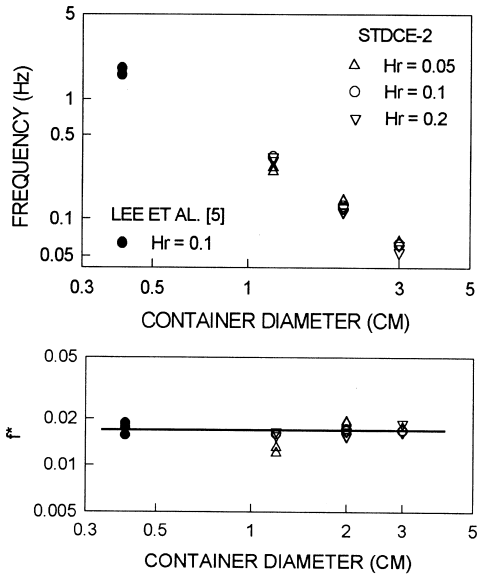

Fig. 9. Dimensional and dimensionless oscillation frequencies for $Ar = 1$.

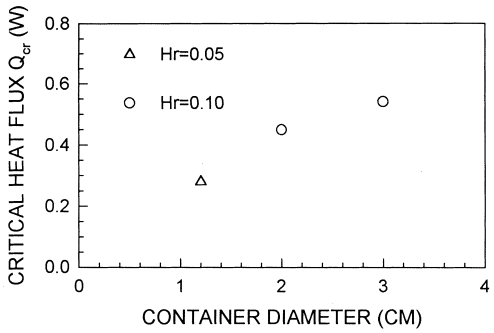

Fig. 10. Critical heat fluxes for $Ar = 0.5$.

The reason for the larger Q_{cr} for $Ar = 0.5$ is that the basic flow is slower for a given flux due to increased effect of the bottom wall. According to the numerical analysis, the maximum stream function is about 70% smaller for $Ar = 0.5$ compared to that for $Ar = 1$ under otherwise the same conditions.

Since it can be shown that the scaling law for the heated region, equation (1), is still valid for $Ar = 0.5$ and that the bulk flow is viscous-dominated, we expect the S-parameter expression, equation (11), to be still true for $Ar = 0.5$. The critical values of S-parameter for $Ar = 0.5$ are shown in Fig. 11. Although not enough data are available, the critical S-parameter seems to be constant ($144 \pm 9\%$) as in the case of $Ar = 1$. Figure 11 also shows the dimensionless oscillation frequencies near the onset of oscillations for $Ar = 0.5$. The value of f^* is nearly constant and close to the value for $Ar = 1$ (Fig. 9).

7. Conclusions

Thermocapillary flow experiments were conducted aboard the Space Shuttle. The flows were generated by CO_2 laser heating in cylindrical containers filled with a high Prandtl number fluid ($Pr = 33$ at 14°C) and became oscillatory beyond the critical heat fluxes. The effects of container dimensions and heating zone size on the oscillation phenomenon were investigated. The critical heat flux increases with increasing container diameter, which is consistent with our ground-based data taken with smaller containers. The effect of heating zone size on the critical flux is relatively small. The Marangoni number alone cannot specify the onset of oscillations, requiring an additional parameter to describe the oscillations. Numerical analysis of the basic flow shows that the bulk flow is viscous-dominated near the onset of oscillations. Therefore, a surface deformation parameter (S-parameter) is derived for the viscous bulk flow. The experimental data show that the flow becomes oscillatory when S is larger than approximately 70 for $Ar = 1$. The oscillation period increases with increasing container diameter and scales with convection time in the bulk flow. Pulsating thermograms are observed during oscillations.

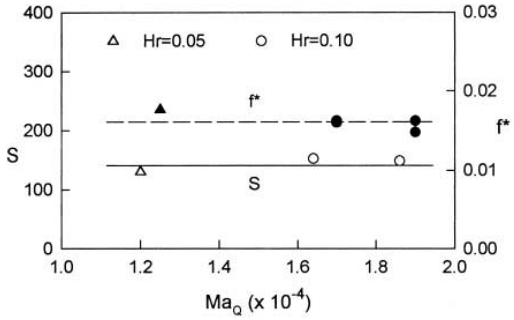

Fig. 11. S-parameter and dimensionless frequency for $Ar = 0.5$.

Acknowledgements

The authors would like to thank many people, especially the NASA Lewis Research Center engineering and operations teams, who worked hard to make the STDCE-2 a successful experiment. Special thanks to the payload crew of the USML-2, Drs Fred Leslie, Kathy Thornton, Cady Coleman and Al Sacco, who conducted the tests expertly to obtain excellent data. The work done at Case Western Reserve University is supported by NASA under grant NAG3-1568.

References

[1] Y. Kamotani, S. Ostrach, A. Pline. Analysis of velocity data taken in surface tension driven convection experiment in microgravity, Physics of Fluids 6 (1994) 3601–3609

[2] Y. Kamotani, S. Ostrach, A. Pline. A thermocapillary convection experiment in microgravity, Journal of Heat Transfer 117 (1995) 611–618.

[3] S. Ostrach, Y. Kamotani. Surface Tension Driven Convection Experiment (STDCE). Contractor Report 198476. NASA, 1996.

[4] A. Pline, R. Zurawski, T. Jacobson, Y. Kamotani, S. Ostrack. Hardware and performance summary of the Surface Tension Driven Convection Experiment-2 aboard the USML-2 Spacelab mission. Paper IAF–96–J.5.01. Presented at the 47th International Astronautical Congress, Beijing, China, 1996.

[5] J.H. Lee, S. Ostrach, Y. Kamotani. A study of oscillatory thermocapillary convection in circular containers with CO_2 laser heating. Report EMAE/TR–94–213. Department of Mechanical and Aerospace Engineering, Case Western Reserve University, Cleveland, OH, 1994.

[6] A. Pline. Surface temperature measurements for the Surface Tension Driven Convection Experiment. Technical Report. NASA TM101353, 1988.

[7] H. Stahl, K. Stultz. Free-surface deformation measurements. AIAA Paper 97–0778. Presented at the 35th AIAA Aerospace Sciences Meeting and Exhibit, Reno, NV, 1997.
[8] Y. Kamotani, A. Chang, S. Ostrach. Effects of heating mode on steady axisymmetric thermocapillary flows in microgravity, Journal of Heat Transfer 118 (1996) 191–197.
[9] Y. Kamotani, S. Ostrach, J. Masud. Conditions for the onset of oscillatory thermocapillary flows in cylindrical containers with CO_2 laser heating. AIAA Paper 97–0889. Presented at the 35th AIAA Aerospace Sciences Meeting and Exhibit, Reno, NV, 1997.
[10] J. Masud, Y. Kamotani, S. Ostrach. Oscillatory thermocapillary flow in cylindrical columns of high Prandtl number fluids, Journal of Thermophysics and Heat Transfer 11 (1997) 105–111.